



This open access document is published as a preprint in the Beilstein Archives with doi: 10.3762/bxiv.2019.58.v1 and is considered to be an early communication for feedback before peer review. Before citing this document, please check if a final, peer-reviewed version has been published in the Beilstein Journal of Nanotechnology.

This document is not formatted, has not undergone copyediting or typesetting, and may contain errors, unsubstantiated scientific claims or preliminary data.

Preprint Title Facile synthesis of Silver nanoparticles with medicinal grass and its biological assessment

Authors Satheshkumar Balu, Swetha Andra, Saranya Kannan, Manisha vidyavathy S and Murugesan Muthalagu

Article Type Full Research Paper

Supporting Information File 1 Consent form.pdf; 680.9 KB

ORCID® iDs Satheshkumar Balu - <https://orcid.org/0000-0003-0012-6212>;
Swetha Andra - <https://orcid.org/0000-0002-2649-4358>; Manisha vidyavathy S - <https://orcid.org/0000-0001-9052-7735>

Facile synthesis of Silver nanoparticles with medicinal grass and its biological assessment

Satheeshkumar Balu¹, Swetha Andra², Saranya Kannan³, Manisha Vidyavathy S^{1*}, Murugesan Muthalagu².

¹*Department of Ceramic Technology, A.C Tech Campus, Anna University, Chennai-600 025, India.*

²*Department of Textile Technology, A.C Tech Campus, Anna University, Chennai-600 025, India.*

³*Department of Chemistry, CEG Campus, Anna University, Chennai- 600 025, India.*

Corresponding Address:

Email: manisha@annauniv.edu

Department of Ceramic Technology,
A.C Tech Campus, Anna University,
Chennai-600 025, India.

Graphical Abstract

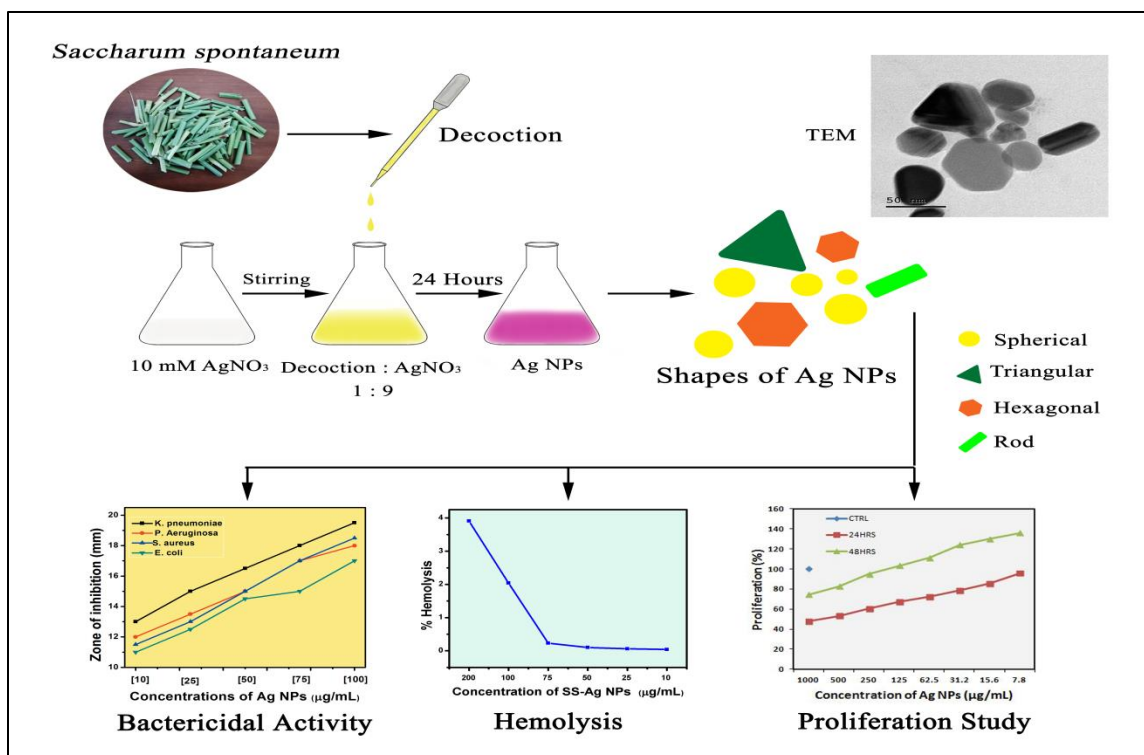


Figure 1: Schematic representation of SS-Ag NPs synthesis and *in-vitro* biological assessment.

Abstract

Biogenic synthesis of silver nanoparticles (SS-Ag NPs) using the extract of *Saccharum spontaneum* (SS) via green chemistry route was investigated for their *in-vitro* cytotoxicity on osteoblast-like cells and bactericidal effect. Synthesized SS-Ag NPs were analyzed using TEM, FTIR, XRD and UV Vis spectroscopy techniques. The biomolecules present in *S. spontaneum* were responsible for the reduction and capping of silver nanoparticles. A heterogeneous mixture of SS-Ag NPs which consists of triangle, hexagonal, spherical and rod-like structures was obtained. Furthermore, the synthesized SS-Ag NPs were tested for in a broad spectrum of antibacterial activity against *E. coli*, *S. aureus*, *K. pneumonia* and *P. aeruginosa* and it showed

significant inhibitory effect. For the first time, the enhancement in the proliferation rate of MG63 cells with SS-Ag NPs is reported.

Keywords: Silver nanoparticles, Biogenic synthesis, Antibacterial, *In-vitro* studies.

1. INTRODUCTION

The demand for nanomaterials is growing more rapidly due to the widespread applications of nanomaterials in various fields including industry, technology and medicine. Among the metallic nanomaterials, silver nanoparticles are widely used in photonics, microelectronics, photocatalysis and antimicrobial treatments [1, 2]. Recently, microbial infections are a major concern in the health care industries, especially for dental and orthopedic implants. Colonization of bacteria on the implants from remote sources can result in the delay of wound healing and finally implant rejection, which actually leads to subsequent implant replacement [3, 4]. As silver is known for its biocidal effect against bacterial and fungal species, it has been widely used as a coating and composite material in implants in order to reduce the biofilm formation [5, 6].

Specifically, the high clearance rate of silver nanoparticles from the body is an advantage of using it in biomedical industry [7]. Recent report reveals that the incorporation of Ag NPs with filler materials gives enhanced activities when compared to the current root canal treatments [8]. Titanium embedded with silver nanoparticles (Ag NPs) experiences microgalvanic effects which enhances antibacterial activity and excellent compatibility with osteoblasts [9]. Several chemical, physical and biological methods have been employed to synthesize silver nanoparticles but are limited in biomedical applications due to the high cost and

usage of hazardous chemicals, harsh solvents and toxic capping agents which cause fatal damage to both environment and humans [10]. Biological synthesis of nanoparticles involves use of bacteria, fungi and plants to produce nanoparticles. Due to the specialized requirements in the maintenance of bacteria and fungi its usage has been limited in the synthesis of nanoparticles [11]. The proteins from fungi and bacteria that act as capping agent may cause allergic reactions. Hence, safe and cost-effective biosynthesis with plants has become an encouraging concept to replace the chemical synthesis in order to eliminate the risk of toxic chemicals and their side effects [12].

Silver nanoparticles are prepared using extracts acquired from various plants including *Thymbra spicata* (leaves), *Boerhaavia diffusa* (whole plant), Turmeric (rhizobium), Green and Black tea (leaves), Cardamom (leaves), *Prosopis juliflora* (bark), *Nyctanthes arbor-tristis* (flower) and *Citrus sinensis* (peel) [13-18]. During the last decade, hundreds of plant extract were effective in the synthesis of silver nanoparticles. The biomolecules present in the plant components such as flavonoids, terpenoids, alkaloids, steroids, saponins and tannins play a major role in the synthesis of nanoparticles [19, 20]. Researchers have reported that the gram-negative bacteria are becoming resistant to silver nanoparticles due to the production of flagellin, which eliminates the antibacterial activity. Hence, the combination of silver nanoparticles with the phytochemical constituents can prevent the aforesaid issues [21].

The present work describes a simple, cost-effective and safe protocol for the preparation of stable silver nanoparticles using aqueous extracts from one of the promising herbal plants *S. spontaneum*. The plant *S. spontaneum* is commonly known as wild sugarcane and is easily available across South Asia, East Africa and Mediterranean [22]. The decoction of the plant

extract is used to treat a variety of diseases such as burning sensation, urinary tract infections, diarrhea, obesity, haemorrhoids and renal calculi. In Ayurvedic medicine, the root decoction of *S. spontaneum* is given for lactating mothers to improve the production of milk [23, 24]. Therefore, the plant extract is extremely safe and suitable for the production of silver nanoparticles by acting as reducing and stabilizing agent. Accordingly, the *S. spontaneum* synthesized silver nanoparticles (SS-Ag NPs) were investigated for its bactericidal effect against both gram-positive and gram-negative bacteria. Furthermore, cell viability and morphology of SS-Ag NPs was carried out using MG63 cell lines.

Metal nanoparticles can be synthesized in different morphologies such as spherical, triangular, rod, hexagonal, wires and cubes by optimizing the parameters such as reaction time, temperature, concentration and pH [25, 26]. Interestingly, Banerjee *et.al.* reported that the shape of the silver nanoparticles is dependent on the reaction time. Initially, spherical nanoparticles were formed which changes to trigonal or rod-shaped [27]. To the best of our knowledge, there are very few reports available for the synthesis of Ag NPs with multiples shapes using plant extracts and for the first time the medicinal plant *S. spontaneum* was used as reducing and capping agent to produce SS-Ag NPs and the MTT assay was performed using MG63 osteoblast-like cells in order to evaluate the cell viability.

2. RESULTS AND DISCUSSIONS

The synthesis of SS-Ag NPs was demonstrated using the *S. spontaneum* and the cytotoxic effect and antibacterial behavior was evaluated.

2.1. Localized Surface Plasmon Resonance Analysis

During synthesis, the formation of SS-Ag NPs was monitored via the solution color change. The colorless solution had changed to yellowish brown and reddish brown after the addition of the plant decoction. The active compounds of the plant decoction reduce the silver ions (Ag^+) into silver nanoparticles (Ag^0). The optical properties of the SS-Ag NPs were correlated with the surface plasmon resonance (SPR) of the excitons. Figure 2 shows the UV-Visible spectra of synthesized SS-Ag NPs at different time intervals such as 0.5, 1, 4, 12, and 24 h. A plasmonic absorbance peak was observed at 464 nm with no significant shifts. The intensity of the peak increased with respect to the increase in reaction time. The formation rate of SS-Ag NPs nanoparticles is directly proportional to the intensity of SPR [28]. Moreover, time-dependent UV spectrum shows the reducing ability of phytochemicals present in the plant decoction. The rate of reaction was initially high, after which it has steadily declined. Until 12 h, the reaction rate was high and after 24 h, it has reached a plateau due to the non-availability of Ag^+ ions. After 24 hours, no major differences were recorded due to the complete reduction of silver ions which indicates phytochemicals took 24 h to completely reduce the Ag^+ ions. However, the reaction time could be possibly reduced by changing the parameters such as temperature, pH, and concentration. Additionally, no visible changes were observed up to 12 months from the synthesized period, which was ascribed to enhanced stability of the SS-Ag NPs [29].



Figure 2: UV-Visible Spectra of SS-Ag NPs synthesized from *S. spontaneum*

2.2. Crystallographic Analysis

X-ray diffraction (XRD) pattern of synthesized material is shown in figure 3 and is found to be well matched with the standard Ag with the JCPDS No 89-3722. The reflection peaks are observed at 38° , 44° , 64° , and 77° corresponding to (1 1 1), (2 0 0), (2 2 0) and (3 1 1) planes indicating the face-centered cubic (FCC) structure of silver. The broad base and sharp tip of the peaks indicate that the material is nanocrystalline. The average nanocrystallite size of the SS-Ag NPs is 10.71 nm with a lattice strain of 0.0104 nm. The broad peak observed around 25° is attributed to the deposition of the phytochemical compounds of *S. spontaneum* on Ag NPs [30-32].

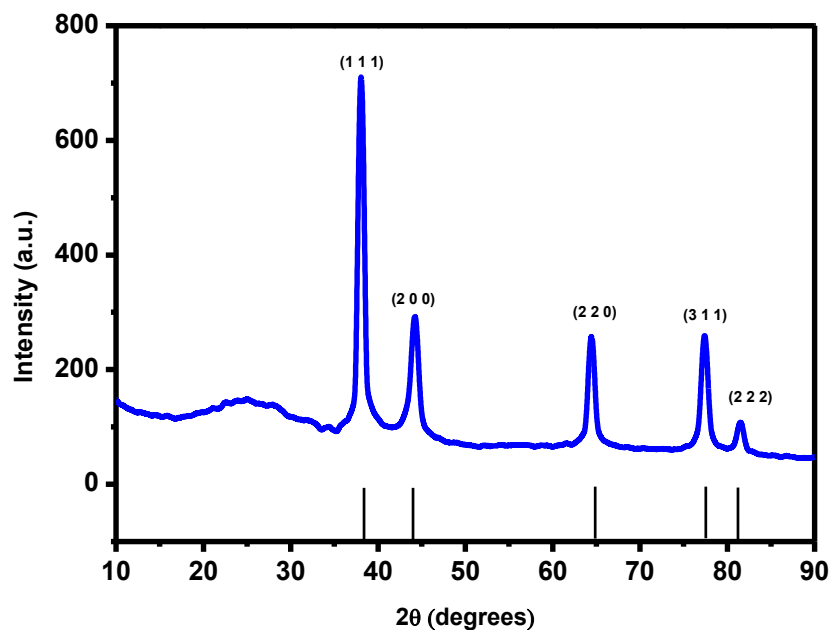


Figure 3: XRD spectrum of SS-Ag NPs synthesized from *S. spontaneum*

2.3. Functional Group Analysis

Figure 4 represents the FTIR spectrum of plant decoction and synthesized SS-Ag NPs of *S. spontaneum*. In this study, the strong broad absorption band at 3385 cm^{-1} indicates the -OH stretching of phenols. The peaks appeared at 2135 and 2137 cm^{-1} corresponds to $\text{C}\equiv\text{C}$ stretching of alkynes [33, 34]. The bands at 1643 and 1650 cm^{-1} represent $\text{C}=\text{O}$ stretching of aldehydes and ketones, respectively. The bands centered at 800 cm^{-1} indicates the $\text{C}-\text{H}$ stretching of alkenes. In most of the studies, phenolic compounds are recognized as the active reducing compounds among other biomolecules [35, 36].

Earlier research studies suggest that phytochemicals such as sugar molecules, amino acids, saccharides, and flavonoids present in the plant extract acts as reducing and capping agents [37, 38]. The major constituent of *S. spontaneum* water extract is polyphenols, quinines,

alkaloids, tannins, carbohydrates, protein, coumarin, steroid and glycosides [39]. There are three stages in the formation mechanism of biogenic Ag NPs: (i) The biomolecules like polyphenols and tannins present in *S. spontaneum* have the ability to reduce and chelate Ag^+ ions due to its strong antioxidant property; (ii) The reduced Ag NPs acts as a nucleation site causing clustering and (iii) leading to nanoparticles formation. The shape and size of the nanoparticles depend on the nature and concentration of the reducing agent, pH, temperature, and concentration of AgNO_3 solution. The presence of polyphenolic compound in SS-Ag NPs indicate that the hydrogen abstraction due to $-\text{OH}$ group of polyphenols induce the reduction of silver ions [40, 41]. The notable peaks of alkynes, aldehydes and ketones group intensity were decreased and C-H vibrations of alkenes groups were shifted from 702 to 800 after the synthesis of SS-Ag NPs and these changes reveals that the biomolecules are oxidized and involved in stabilization process [42]. The IR results confirm the stabilization of SS-Ag NPs with the biomolecules through the coordination of the carbonyl group and oxidized polyphenol [43]. The stability of prepared SS-Ag NPs is determined by the nature of the biomolecules involved in the capping process [44]. In conclusion, biomolecules present in the plant decoction actively participate in the reduction and capping process.

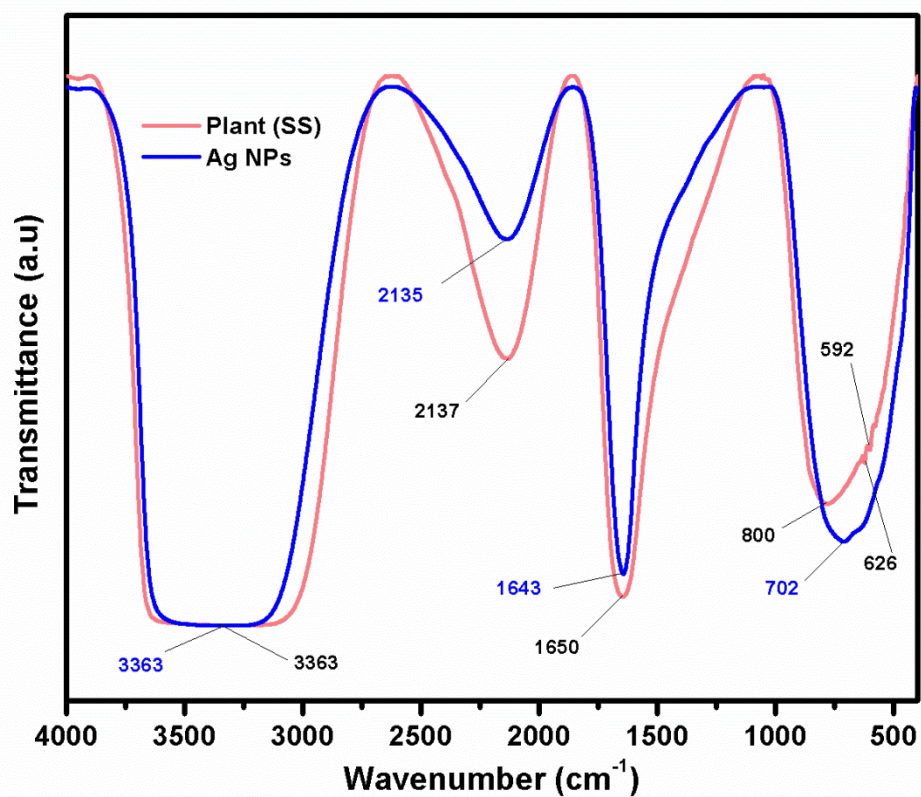


Figure 4: FTIR spectra of the plant decoction and synthesized SS-Ag NPs of *S. spontaneum*

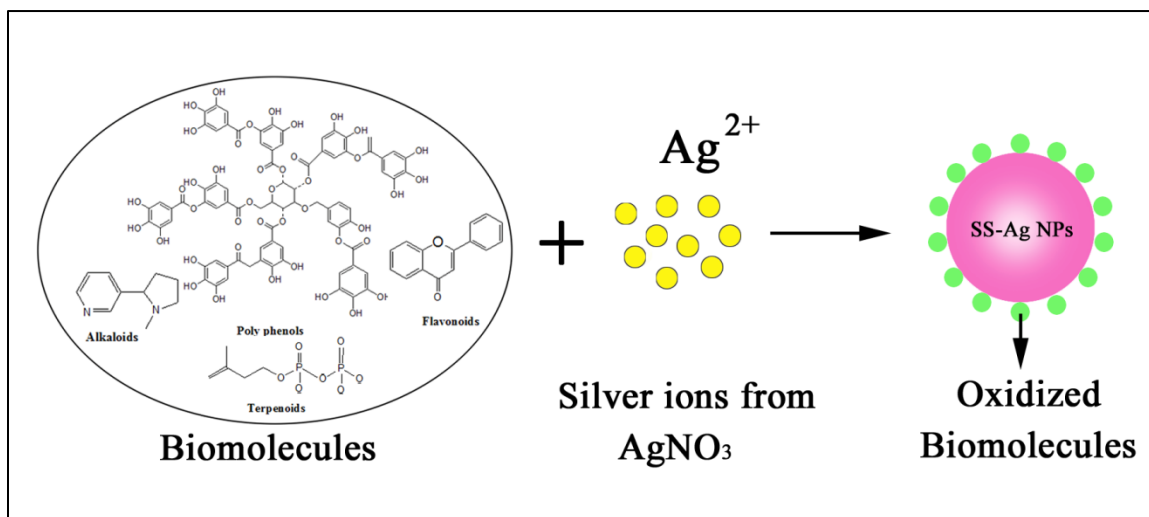


Figure 5: Proposed mechanism of SS-Ag NPs formation

2.4. Transmission Electron Microscope

The transmission electron microscopic image reveals the different morphologies of synthesized SS-Ag NPs as shown in figure 6. The TEM images show a mixture of silver nanoparticles with different sizes ranging from 10 to 100 nm and most of the particles lie in the range of 30-40 nm. Spherical, triangular, rod and hexagonal shaped silver nanoparticles were observed. It could be essentially due to the differences in the binding habit of different functional groups present in the SS extracts [45, 46]. Among the various shapes of SS-Ag NPs, the spherical nanoparticles were predominant and these nanoparticles have multiple applications in the biomedical field. The crystallinity of the SS-Ag NPs was analyzed using selected area diffraction (SAD) and the selected area electron diffraction (SAED) pattern is given in figure 6(e). The appearance of several small points indicates that the nanocrystals are oriented in different directions which suggest the polycrystalline nature of the synthesized SS-Ag NPs. The interplanar distance was determined by the diffraction rings pattern and was estimated to be 2.3, 2.04, 1.39 and 1.27 nm which were consistent with the face-centered cubic structure of silver nanoparticles [47].

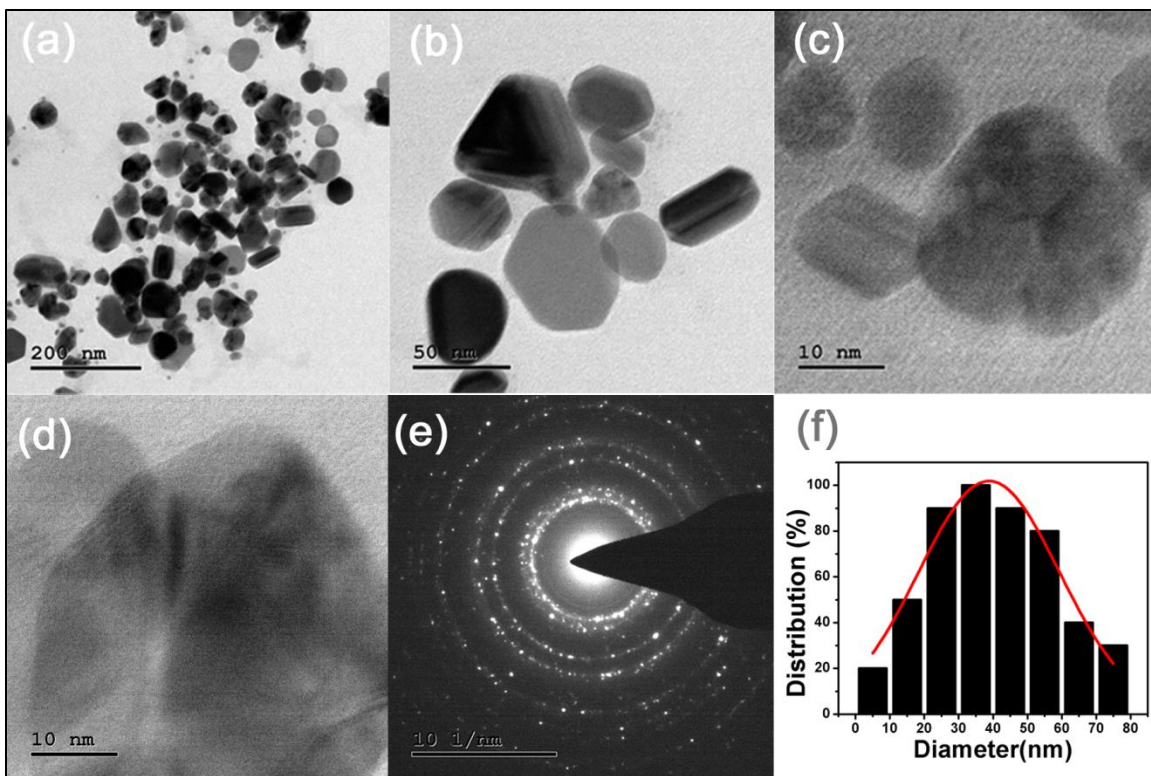


Figure 6: TEM images of SS-Ag NPs in different magnification (a-d), SAED pattern of SS-Ag NPs (e), and Particle Size distribution (f).

2.5. DLS and zeta potential

The diameter of synthesized Ag NPs nanoparticles determines their bioactivity such as cytocompatibility, bactericidal activity and hemo compatibility. The obtained DLS curve shows the size distribution of SS-Ag NPs with average size 80 nm and polydispersity index (PDI) is 0.886 which indicates nanoparticles were poly-dispersed [48, 49]. The observed size distribution of SS-Ag NPs by DLS and TEM found to be 80.66 nm and 39.6 nm respectively. The variation in size is due to that, the DLS measures the size of the core NPs along with biomolecules attached on the surface, whereas TEM measures the actual of the Ag NPs. The stability of the colloidal NPs can be predicted by measuring the electrostatic attractive and repulsive forces

between the NPs using zeta potential (ζ). The obtained ζ potential curve reveals that the average zeta potential value is 41.32 mV which means that the formed Ag NPs is highly stable due to the positive-positive repulsion [50, 51].

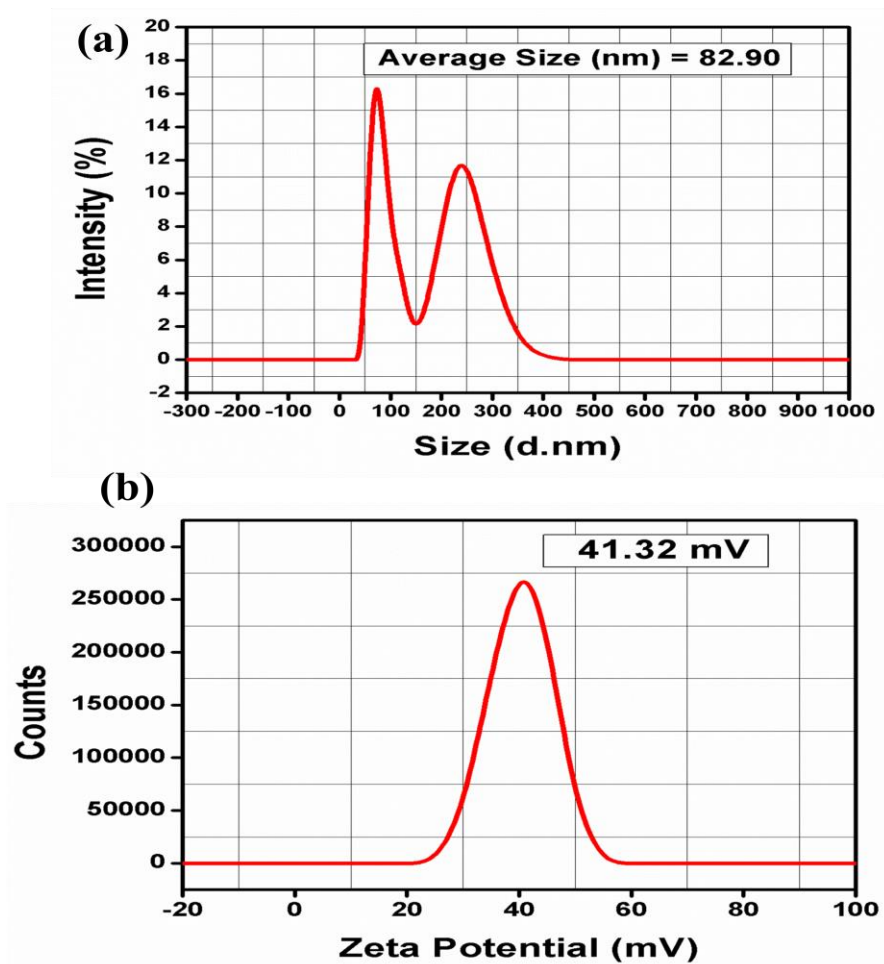


Figure 7: DLS particle size distribution (a), Zeta potential of colloidal SS- Ag NPs (b)

2.6. Antimicrobial activity

Gram-negative bacteria are the major cause of nosocomial infections due to their inherent resistance for antibiotics. Biogenically synthesized SS-Ag NPs antimicrobial activity was examined against the gram-negative (*E. coli*, *P. aeruginosa* and *K. pneumonia*) and gram-

positive bacteria (*S. aureus*). The obtained results are displayed in figure 8(a). From the results, it was inferred that the zone of inhibition was increased with increasing concentration of the SS-Ag NPs. However, there was no much change in the zone diameter for 100 µg/mL as compared with 75 µg/mL. The antibacterial activity of SS-Ag NPs against gram-negative bacteria was more than gram-positive bacteria due to the variations in peptidoglycan layer thickness [52]. Among the various bacterial strains, the SS-Ag NPs showed enhanced antimicrobial activity against *K. pneumoniae* (figure 8b) due to the variations in cell structure, diffusion rate, metabolism and interaction of the nanoparticles with the microorganisms [53].

The mechanism behind the antimicrobial activity of SS-Ag NPs might involve (i) the binding of silver cations to the negatively charged bacterial cell wall causing cell rupture and finally the cell death, (ii) the silver nanoparticles penetrate the bacterial cell wall and interacts with the cellular biomolecules causing irreversible damage, (iii) the generation of free radical of reactive oxygen species (ROS) induced by metals/metal oxides might have interacted with bacterial membrane and resulted in the oxidative stress, and (iv) the Ag⁺ ions released from the silver nanoparticles binds with the purines and pyridines, thereby disrupting the bacterial reproduction [54-56].

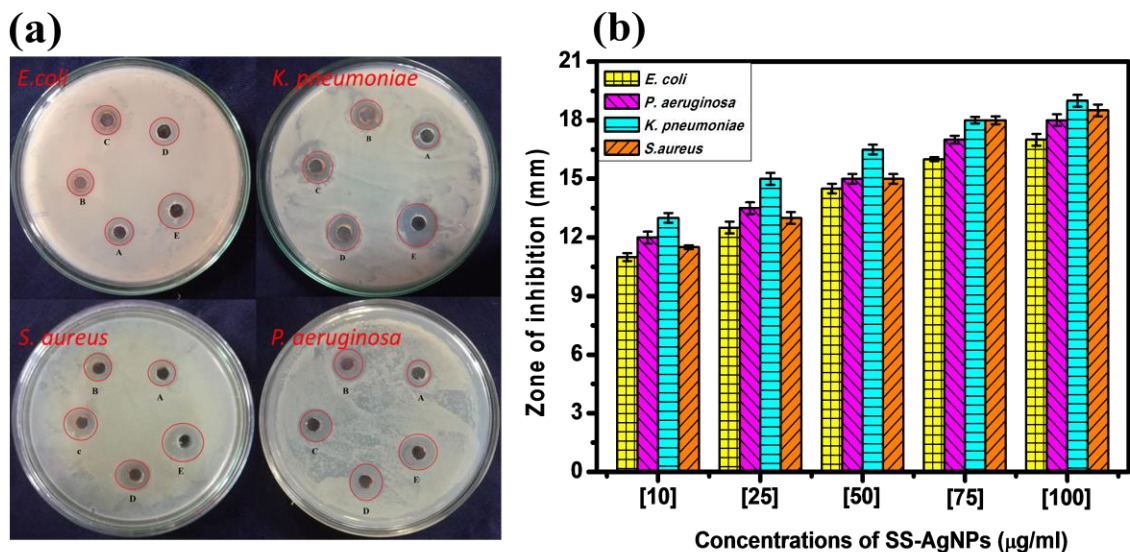


Figure 8: Antimicrobial activity of SS-Ag NPs

2.7. Hemolysis

The hemolytic activity of the SS-Ag NPs was investigated at various concentrations and the obtained results were calculated and correlated with ASTM (American Society for Testing and Materials) standard F756-00. Until 75 µg/ mL, SS-Ag NPs exhibits less than 2 % of hemolysis, which indicates that the material is completely non-hemolytic. At the concentration of 100 and 200 µg/mL the hemolytic percentage was approximately 2 and 4.5 which indicates that the material exhibits slightly hemolytic behavior.

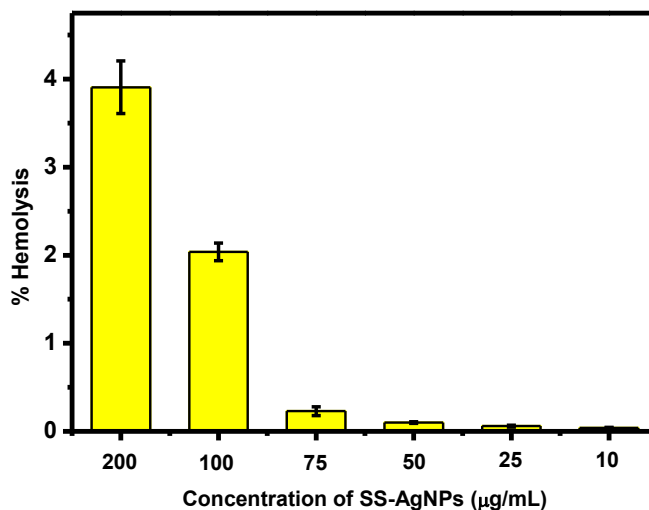


Figure 9: Hemolytic behavior of SS-Ag NPs at various concentrations

2.8. MTT Assay

The effect of SS-Ag NPs on the proliferation rate of MG63 cell line was evaluated using MTT Assay. The test was performed after culturing the cells for 24 and 48 h in the presence of the synthesized SS-Ag NPs at different concentrations (7.8, 15.6, 31.2, 62.5, 125, 250, 500 and 1000 µg/mL) and the relative percentage cell viability was plotted graphically to measure the proliferation efficacy of the cells (figure 10). After 24 h of incubation, as the concentrations of SS-Ag NPs increases from 7.8 to 1000 µg/mL, the cell viability decreases from 95 to 48 %. Until 125 µg/mL of SS-Ag NPs, there is no cytotoxicity as the cell activity was approximately 70 % [57]. However, after 48 hours, the percentage of cell viability was increased up to 135 % above the control in lower concentrations [58, 59]. As the concentration of SS-Ag NPs increases, the proliferation rate decreases. At 1000 µg/mL, the proliferation rate was similar to the control. Initially, the immediate exposure of Ag NPs at high concentrations has led to cell death. As the incubation time increases, the concentration of the silver ions decreases and attains a favorable

concentration that enhances the proliferation of the MG63 cells. At lower concentrations, the Ag^+ ions enter the cells and bind with the DNA thereby activating the gene expression of HIF-1 α and IL-8 which enhances the cell proliferation rate. In addition, the Ag^+ ions have the ability to attract the mesenchymal and fibroblast cells leading to faster healing of bone fractures [60].

Similarly, the effect of SS-Ag NPs on the morphological changes in the cell lines was studied through an optical microscope and the obtained images are displayed in figure 10(b). The histogram (figure 10(a)) shows drastic proliferation of cells in 48 h than 24 h and similar results were also found by the optical images, which showed that the cell growth was visibly seen after 48 h as compared to 24 h. This could be explained as follows. As observed from the TEM images, the dispersed colloidal solution contains four shapes of nanoparticles, and especially, the nanorods of Ag can easily enter into the cytoplasm owing to their one-dimensional shape and as well as the increased incubation time [61, 62]. These findings further suggest that internalization of nanoparticles or incubation time could have changed the morphology of the cells without affecting their proliferation. However, further studies should be done to interpret other biological activities.

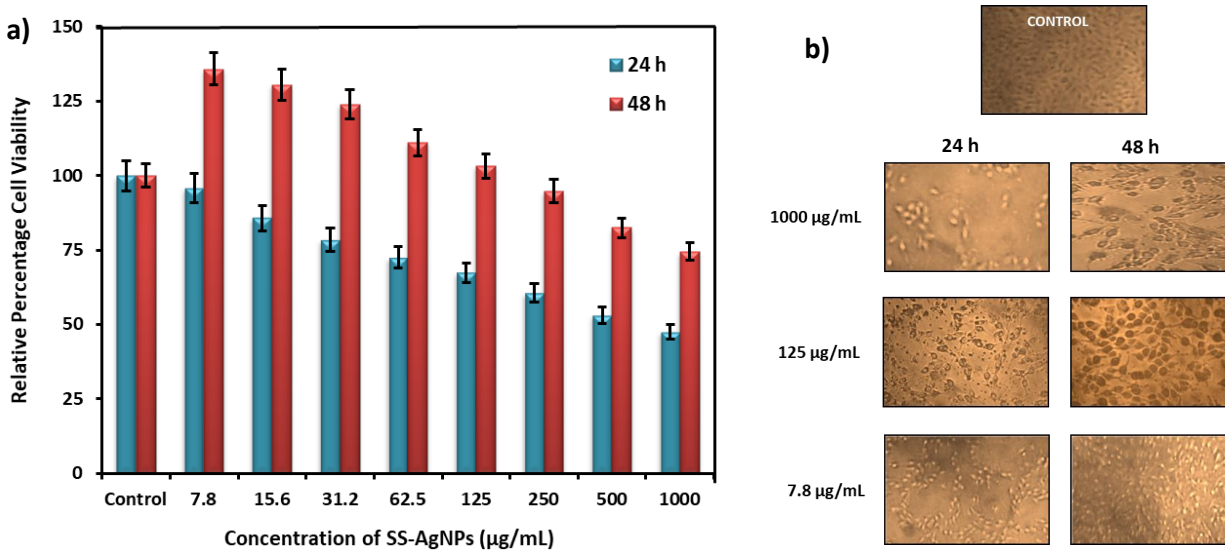


Figure 10: Effects of SS-Ag NPs on the viability of MG-63 cells. (a) The viability of MG63 cells treated with different concentrations of SS-Ag NPs for 24 and 48 h by MTT Assay and (b) the treated cells were visualized under an optical microscope.

3. Conclusion

In the present work, different shapes of silver nanoparticles were synthesized biogenically using medicinal plant *S. spontaneum* plant decoction as a reducing-cum-stabilizing agent. The SS-Ag NPs exhibited surface plasmon resonance peak at 464 nm and face-centered crystallographic structure with the crystallite size of 10.8 nm. FTIR analysis revealed the stretching and bending vibration of alkenes and carbonyl groups were shifted indicating that the oxidation of the biomolecules led to the formation of SS-Ag NPs. The TEM micrograph showed the existence of various shapes of SS-Ag NPs namely spherical, triangular, rod and hexagonal shapes. The particle sizes were measured using DLS and the results showed that the synthesized nanoparticles had various sizes ranging from 10 to 300 nm. The prepared material was non-hemolytic till 75 µg/mL, after which it was slightly hemolytic. Cell proliferation assay was

performed using MG63 cells and the observed results revealed that the proliferation rate of cells has significantly increased based on dose-dependent manner. At lower concentration of SS-Ag NPs, the proliferation rate was increased by 35 % whereas, at higher concentrations, the proliferation rate was similar. Therefore, the SS-Ag NPs could be used till 1000 $\mu\text{g/mL}$. However, the morphology of MG63 has changed significantly at 125 $\mu\text{g/mL}$. An improved antimicrobial activity was also observed by zone of inhibition studies and these findings suggest that the synthesized SS-Ag NPs have significant antimicrobial activity at 75 $\mu\text{g/mL}$ and upon further increase in concentration, no significant change was observed. On the whole, the prepared SS-Ag NPs at the concentration of 75 $\mu\text{g/mL}$ could be an effective dosage for bone implants for faster wound healing with good antimicrobial activity.

4. EXPERIMENTAL PROCEDURE

4.1 Preparation of Plant Decoction

Fresh *Saccharum spontaneum* plant stems was collected from Ramanathapuram district, India. The outer layer of the stems was removed and young stems were washed with tap water followed by distilled water to remove the dust particles from the surface. Sliced stems were crushed well with electric mixer-grinder and they were added to distilled water in a ratio (w/v) 1:10. The mixture was boiled at 50 °C for 30 min to get the plant extract and allowed to cool at room temperature and filtered through Whatman no 1 filter paper to get the plant decoction. The obtained decoction was stored at a brown bottle and kept in the refrigerator at 4 °C for future experiments.

4.2 Preparation of Silver nanoparticles (SS-Ag NPs)

For SS-Ag NPs synthesis, 10 mL of plant decoction was added dropwise to 90 mL of 10 mM AgNO₃ solution under constant stirring at room temperature. Then the solution was centrifuged at 10,000 rpm for 15 min. The obtained precipitate was washed thrice with distilled water to remove the unbound extracts. The precipitate was finally dried and used for further characterizations.

4.3 Characterization of SS-Ag NPs

The optical absorbance of UV-Visible spectroscopy was recorded using Hitachi, model U-3900, Japan. The colloidal solution of SS-Ag NPs was analyzed in the spectral region from 300 to 700 nm wavelength. The crystallinity of the SS-Ag NPs was evaluated using X-ray powder diffraction Bruker, model D8 Advance. Fourier Transform Infrared Spectroscopy (FTIR, Perkin Elmer spectrum model Spectrum one) was used to identify the functional groups in the prepared extract and SS-Ag NPs. The samples were scanned from 4000 to 500 cm⁻¹.

A drop of SS-Ag NPs solution was placed on the carbon-coated copper grid and allowed to dry completely. The shapes and size of the synthesized nanoparticles were observed using Transmission electron microscope (TEM, JEOL Japan). Particle size distribution and ζ- potential analysis was performed using Zeta sizer (Malvern Instruments, Malvern, UK). SS-Ag NPs were dispersed well in the distilled water using ultra sonicator for 30 min and samples were fed into the instrument and the graphs were recorded.

4.4 Antimicrobial Studies

The antimicrobial activity of SS-Ag NPs was investigated using Well diffusion method. The pure cultures of the bacteria (*E. coli*, *S. aureus*, *P. aeruginosa* and *K. Pneumoniae*) were

obtained from the National Centre for Microbial Resource (NCMR, Pune). The bacterial pathogens were cultivated in Nutrient Agar (SRL Chemicals, India). The sterilized nutrient agar was poured into a petridish and the fresh microbial cultures were spread over the agar using sterile cotton swabs. Wells was formed by puncturing the nutrient agar using sterile micropipette tip. The SS-Ag NPs was added to the wells in various concentrations viz.10, 25, 50, 75 and 100 μ L. The plates were incubated for 24 hours at 37 °C and the zone of inhibition was measured. Finally, the microbes were properly discarded using an autoclave to prevent the environment from contamination.

4.5 Hemolysis Assay

Human blood was taken from the volunteer with the help of clinicians. The experiments were conducted in accordance with the relevant laws and institutional guidelines. The informed consent was obtained from the blood donor for the assay. The blood was mixed with 3.2% of trisodium citrate in the ratio 1:10 to prevent coagulation. The different concentrations (200, 100, 75, 50, 25 and 10 μ g/mL) of the SS-Ag NPs were prepared with phosphate buffered saline (PBS) and anticoagulated blood served as the test specimen. Anti-coagulated blood with 0.1% sodium carbonate and PBS with anticoagulated blood were used as the positive and negative control, respectively. All the samples and the controls were incubated at 37 °C for 3 h. Then, the tubes were centrifuged at 2000 rpm for 5 min. The optical density (OD) of the supernatant was measured at 545 nm [63]. All the tests were done thrice to ensure the reproducibility. The percentage of hemolysis was calculated as,

$$\text{Hemolysis (\%)} = \frac{(\text{Absorbance of test sample} - \text{Absorbance of negative control})}{(\text{Absorbance of positive control} - \text{Absorbance of negative control})} \times 100$$

4.6 Biocompatibility assessment of SS-Ag NPs

The biocompatibility of biosynthesized SS-Ag NPs should be justified using *in vitro* studies before intended with *in vivo*. Accordingly, the cytocompatibility and proliferation of MG63 cell lines were analyzed with SS-Ag NPs. MG63 osteoblast-like cell line was obtained from National Centre for Cell Sciences (NCCS, Pune). Dulbecco's modified Eagle's medium (DMEM) with 10% fetal bovine serum (FBS), penicillin (100 U/mL) and streptomycin (100 µg/mL) was used to maintain the culture in humidity atmosphere of 50 µg/mL CO₂ at 37 °C. Approximately 1 × 10⁵/well MG63 cells were seeded in 24 well plates and incubated under CO₂ condition at 37 °C. The synthesized SS-Ag NPs were added in various concentrations such as 1000, 500, 250, 125, 62.5, 31.2, 15.6, 7.8 µg/mL and incubated at 37 °C for 24, 48 and 72 h.

MTT assay was performed to determine the cytotoxic behavior of the SS-Ag NPs. 3-(4,5-dimethylthiazol-2-yl)-2,5-diphenyl tetrazolium bromide (MTT) was added with the cells and incubated for 4 h. 1 mL of dimethyl sulphoxide (DMSO) was added to dissolve the formazan crystals and the optical density values were measured at 570 nm using ELISA reader (Bio-Rad 680, USA) [64]. The assay was performed in triplicate and the percentage of cell viability was calculated using the following formula.

$$\text{Cell Viability (\%)} = (A_{570} \text{ of treated cells}) / (A_{570} \text{ of control cells}) \times 100$$

The cells incubated with different concentration of SS-Ag NPs were fixed with 4% paraformaldehyde and then visualized using an optical microscope.

5. Acknowledgement

The authors would like to thank the head of the Department of Animal Biotechnology for utilizing biocompatibility assessment facilities at TANUVAS, Veppery, Chennai-07.

6. References

- 1.A. Rónavári, D. Kovács, N. Igaz, C. Vágvölgyi, I.M. Boros, Z. Kónya, I. Pfeiffer, M. Kiricsi, *International journal of nanomedicine*, 12 (2017) 871.
- 2.M. Gomathi, P. Rajkumar, A. Prakasam, K. Ravichandran, *Resource-Efficient Technologies*, 3 (2017) 280-284.
- 3.C.R. Arciola, D. Campoccia, L. Montanaro, *Nature Reviews Microbiology*, (2018) 1.
- 4.Z. Khatoon, C.D. McTiernan, E.J. Suuronen, T.-F. Mah, E.I. Alarcon, *Heliyon*, 4 (2018) e01067.
- 5.C.Y. Flores, A.G. Miñán, C.A. Grillo, R.C. Salvarezza, C. Vericat, P.L. Schilardi, *ACS applied materials & interfaces*, 5 (2013) 3149-3159.
- 6.J. Lee, W. Murphy, in: *Annual Meeting of the Orthopaedic Research Society*, San Francisco, CA, 2012.
- 7.J.H. Lee, Y.S. Kim, K.S. Song, H.R. Ryu, J.H. Sung, J.D. Park, H.M. Park, N.W. Song, B.S. Shin, D. Marshak, *Particle and fibre toxicology*, 10 (2013) 36.
- 8.E. Ertem, B. Gutt, F. Zuber, S. Allegri, B. Le Ouay, S. Mefti, K. Formentin, F. Stellacci, Q. Ren, *ACS applied materials & interfaces*, 9 (2017) 34762-34772.
- 9.H. Cao, X. Liu, F. Meng, P.K. Chu, *Biomaterials*, 32 (2011) 693-705.
- 10.H. Duan, D. Wang, Y. Li, *Chemical Society Reviews*, 44 (2015) 5778-5792.
- 11.S.A. Brennan, C. Ní Fhoghlú, B. Devitt, F. O'mahony, D. Brabazon, A. Walsh, *The bone & joint journal*, 97 (2015) 582-589.
- 12.U. Anjaneyulu, V. Swaroop, U. Vijayalakshmi, *RSC Advances*, 6 (2016) 10997-11007.
- 13.H. Veisi, S. Azizi, P. Mohammadi, *Journal of cleaner production*, 170 (2018) 1536-1543.
- 14.F.K. Alsammarraie, W. Wang, P. Zhou, A. Mustapha, M. Lin, *Colloids and Surfaces B: Biointerfaces*, 171 (2018) 398-405.
- 15.M.A. Asghar, E. Zahir, S.M. Shahid, M.N. Khan, M.A. Asghar, J. Iqbal, G. Walker, *LWT*, 90 (2018) 98-107.
- 16.V. Soshnikova, Y.J. Kim, P. Singh, Y. Huo, J. Markus, S. Ahn, V. Castro-Aceituno, J. Kang, M. Chokkalingam, R. Mathiyalagan, *Artificial cells, nanomedicine, and biotechnology*, 46 (2018) 108-117.
- 17.G. Arya, R.M. Kumari, N. Gupta, A. Kumar, R. Chandra, S. Nimesh, *Artificial cells, nanomedicine, and biotechnology*, 46 (2018) 985-993.
- 18.P. Jamdagni, P. Khatri, J. Rana, *Journal of King Saud University-Science*, 30 (2018) 168-175.
- 19.D.M. Arboleda, J.M. Santillán, V.B. Arce, M.B.F. van Raap, D. Muraca, M.A. Fernández, R.M.T. Sanchez, D.C. Schinca, L.B. Scaffardi, *Materials Characterization*, 140 (2018) 320-332.
- 20.K. Paulkumar, G. Gnanajobitha, M. Vanaja, M. Pavunraj, G. Annadurai, *Advances in Natural Sciences: Nanoscience and Nanotechnology*, 8 (2017) 035019.
- 21.A. Panáček, L. Kvítek, M. Smékalová, R. Večeřová, M. Kolář, M. Röderová, F. Dyčka, M. Šebela, R. Pucek, O. Tomanec, *Nature nanotechnology*, 13 (2018) 65.
- 22.A. Cheavegatti-Gianotto, H.M.C. de Abreu, P. Arruda, J.C. Bessalho Filho, W.L. Burnquist, S. Creste, L. di Ciero, J.A. Ferro, A.V. de Oliveira Figueira, T. de Sousa Filgueiras, *Tropical plant biology*, 4 (2011) 62-89.
- 23.K. Mikawlawng, S. Kumar, R. Vandana, *International Journal of Herbal Medicine*, 2 (2014) 1-12.
- 24.F.A. Ripa, M. Haque, M. Imran-Ul-Haque, *Eur J Sci Res*, 30 (2009) 478-483.
- 25.M. Yilmaz, H. Turkdemir, M.A. Kilic, E. Bayram, A. Cicek, A. Mete, B. Ulug, *Materials Chemistry and Physics*, 130 (2011) 1195-1202.
- 26.G. Martinez-Castanon, N. Nino-Martinez, F. Martinez-Gutierrez, J. Martinez-Mendoza, F. Ruiz, *Journal of Nanoparticle Research*, 10 (2008) 1343-1348.

- 27.S. Banerjee, K. Loza, W. Meyer-Zaika, O. Prymak, M. Epple, *Chemistry of Materials*, 26 (2014) 951-957.
- 28.M. Khan, M. Khan, S.F. Adil, M.N. Tahir, W. Tremel, H.Z. Alkhatlan, A. Al-Warthan, M.R.H. Siddiqui, *International journal of nanomedicine*, 8 (2013) 1507.
- 29.L. Ortega-Arroyo, E.S. Martin-Martinez, M.A. Aguilar-Mendez, A. Cruz-Orea, I. Hernandez-Pérez, C. Glorieux, *Starch-Stärke*, 65 (2013) 814-821.
- 30.V. Lavakumar, K. Masilamani, V. Ravichandiran, N. Venkateshan, D. Saigopal, C.A. Kumar, C. Sowmya, *Chemistry Central Journal*, 9 (2015) 42.
- 31.A.M. Awwad, N.M. Salem, A.O. Abdeen, *International journal of industrial chemistry*, 4 (2013) 29.
- 32.M. Vanaja, G. Annadurai, *Applied Nanoscience*, 3 (2013) 217-223.
- 33.K. Elumalai, S. Velmurugan, *Applied Surface Science*, 345 (2015) 329-336.
- 34.T.N. Jebakumar Immanuel Edison, M.G. Sethuraman, *ACS Sustainable Chemistry & Engineering*, 1 (2013) 1326-1332.
- 35.J. Huang, G. Zhan, B. Zheng, D. Sun, F. Lu, Y. Lin, H. Chen, Z. Zheng, Y. Zheng, Q. Li, *Industrial & Engineering Chemistry Research*, 50 (2011) 9095-9106.
- 36.S. Kummara, M.B. Patil, T. Uriah, *Biomedicine & Pharmacotherapy*, 84 (2016) 10-21.
- 37.M. Nasrollahzadeh, F. Ghorbannezhad, Z. Issaabadi, S.M. Sajadi, *The Chemical Record*, 19 (2019) 601-643.
- 38.M. Nasrollahzadeh, M. Atarod, M. Sajjadi, S.M. Sajadi, Z. Issaabadi, *Plant-Mediated Green Synthesis of Nanostructures: Mechanisms, Characterization, and Applications*, in: *Interface Science and Technology*, Elsevier, 2019, pp. 199-322.
- 39.C. Kumar, R. Varadharajan, P. Muthumani, R. Meera, P. Devi, B. Kameswari, *International Journal of PharmTech Research*, 2 (2010) 319-321.
- 40.S. Ferraris, M. Miola, A. Cochis, B. Azzimonti, L. Rimondini, E. Prenesti, E. Vernè, *Applied Surface Science*, 396 (2017) 461-470.
- 41.E. Rodríguez-León, R. Iñiguez-Palomares, R.E. Navarro, R. Herrera-Urbina, J. Tánori, C. Iñiguez-Palomares, A. Maldonado, *Nanoscale Research Letters*, 8 (2013) 318.
- 42.N. Aziz, M. Faraz, R. Pandey, M. Shakir, T. Fatma, A. Varma, I. Barman, R. Prasad, *Langmuir*, 31 (2015) 11605-11612.
- 43.A. Jeevika, R. Sarika, D.R. Shankaran, *Adv. Mater. Lett.*, 7 (2016) 1021-1028.
- 44.P. Logeswari, S. Silambarasan, J. Abraham, *Scientia Iranica*, 20 (2013) 1049-1054.
- 45.B. Khodashenas, H.R. Ghorbani, *Arabian Journal of Chemistry*, (2015).
- 46.F.F. Soleimani, T. Saleh, S.A. Shojaosadati, R. Poursalehi, *BioNanoScience*, 8 (2018) 72-80.
- 47.A. Hebeish, M. El-Rafie, M. El-Sheikh, M.E. El-Naggar, *Journal of Nanotechnology*, 2013 (2013).
- 48.K. Jyoti, M. Baunthiyal, A. Singh, *Journal of Radiation Research and Applied Sciences*, 9 (2016) 217-227.
- 49.H. Ardani, C. Imawan, W. Handayani, D. Djuhana, A. Harmoko, V. Fauzia, in: *IOP Conference Series: Materials Science and Engineering*, IOP Publishing, 2017, pp. 012056.
- 50.K. Jadhav, S. Deore, D. Dhamecha, S. Jagwani, S. Jalalpure, R. Bohara, *ACS Biomaterials Science & Engineering*, 4 (2018) 892-899.
- 51.A. Saeb, A.S. Alshammari, H. Al-Brahim, K.A. Al-Rubeaan, *The Scientific World Journal*, 2014 (2014).
- 52.T. Chatterjee, B.K. Chatterjee, D. Majumdar, P. Chakrabarti, *Biochimica et Biophysica Acta (BBA)-General Subjects*, 1850 (2015) 299-306.
- 53.S. Andra, R. Ramoorthy, M. Muthalagu, *Materials Research Express*, 5 (2018) 065043.
- 54.V. Dhand, L. Soumya, S. Bharadwaj, S. Chakra, D. Bhatt, B. Sreedhar, *Materials Science and Engineering: C*, 58 (2016) 36-43.

- 55.H.M. Ibrahim, *Journal of Radiation Research and Applied Sciences*, 8 (2015) 265-275.
- 56.C. You, C. Han, X. Wang, Y. Zheng, Q. Li, X. Hu, H. Sun, *Molecular biology reports*, 39 (2012) 9193-9201.
- 57.S.-Y. Chen, M.-T. Huang, S.L. Pender, M. Ruslin, H.-H. Chou, K.-L. Ou, *Materials Science and Engineering: C*, 80 (2017) 624-630.
- 58.V. Gopinath, S. Priyadarshini, M.F. Loke, J. Arunkumar, E. Marsili, D. MubarakAli, P. Velusamy, J. Vadivelu, *Arabian journal of chemistry*, 10 (2017) 1107-1117.
- 59.C.E. Albers, W. Hofstetter, K.A. Siebenrock, R. Landmann, F.M. Klenke, *Nanotoxicology*, 7 (2013) 30-36.
- 60.R. Zhang, P. Lee, V.C. Lui, Y. Chen, X. Liu, C.N. Lok, M. To, K.W. Yeung, K.K. Wong, *Nanomedicine: Nanotechnology, Biology and Medicine*, 11 (2015) 1949-1959.
- 61.J. Jeevanandam, Y. San Chan, Y.H. Ku, *Applied Biological Chemistry*, 61 (2018) 197-208.
- 62.Y. Cai, Y. Liu, W. Yan, Q. Hu, J. Tao, M. Zhang, Z. Shi, R. Tang, *Journal of Materials Chemistry*, 17 (2007) 3780-3787.
- 63.K. Saranya, S.T.K. Raja, R. Subhasree, A. Gnanamani, S.K. Das, N. Rajendran, *Ceramics International*, 43 (2017) 11569-11579.
- 64.K. Saranya, M. Kalaiyarasan, S. Chatterjee, N. Rajendran, *Materials and Corrosion*, 70 (2019) 698-710.